analytical chemistry

pubs.acs.org/ac

Article

Aptamer Sandwich Lateral Flow Assay (AptaFlow) for Antibody-Free SARS-CoV-2 Detection

Lucy F. Yang, Nataly Kacherovsky, Nuttada Panpradist, Ruixuan Wan, Joey Liang, Bo Zhang, Stephen J. Salipante, Barry R. Lutz, and Suzie H. Pun*

Cite This: *Anal. Chem.* 2022, 94, 7278–7285

Read Online

ACCESS | Metrics & More | Article Recommendations | Supporting Information

ABSTRACT: The COVID-19 pandemic is among the greatest health and socioeconomic crises in recent history. Although COVID-19 vaccines are being distributed, there remains a need for rapid testing to limit viral spread from infected individuals. We previously identified the SARS-CoV-2 spike protein N-terminal domain (NTD) binding DNA aptamer 1 (SNAP1) for detection of SARS-CoV-2 virus by aptamer−antibody sandwich enzyme-linked immunoassay (ELISA) and lateral flow assay (LFA). In this work, we identify a new aptamer that also binds at the NTD, named SARS-CoV-2 spike protein NTD-binding DNA aptamer 4 (SNAP4). SNAP4 binds with high affinity (<30 nM) for the SARS-CoV-2 spike protein, a 2-fold improvement over SNAP1. Furthermore, we utilized both SNAP1 and SNAP4 in an aptamer sandwich LFA (AptaFlow), which detected SARS-CoV-2 UV-inactivated virus at concentrations as low as 10^6 copies/mL. AptaFlow costs <$1 per test to produce, provides results in <1 h, and detects SARS-CoV-2 at concentrations that indicate higher viral loads and a high probability of contagious transmission. AptaFlow is a potential approach for a low-cost, convenient antigen test to aid the control of the COVID-19 pandemic.

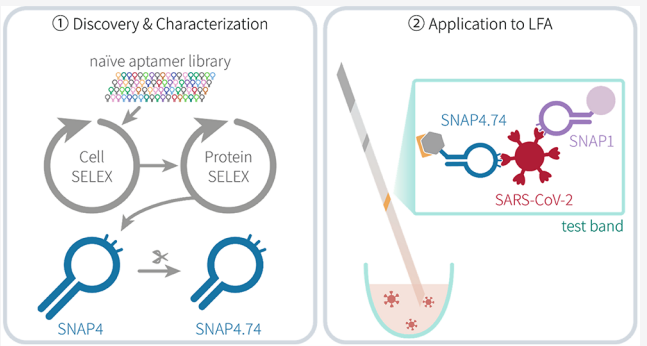

The coronavirus disease 2019 (COVID-19) pandemic is one of the largest public health threats to date. Although COVID-19 vaccines have been authorized and administered to almost 4 billion people worldwide, vaccine dissemination remains a challenge,[1] and new variants of concern (VOCs) with increased transmissibility, severity, or vaccine escape capabilities continue to develop. Preventative measures, including frequent testing, are needed in addition to vaccines to control COVID-19.

Among COVID-19 diagnostics, rapid antigen tests for SARS-CoV-2 are important tools for curbing the pandemic.[2] Rapid antigen tests are inexpensive to produce and provide point-of-care results. Users can make better-informed risk decisions through more frequent testing, even if they are less sensitive.[3,4] In this manner, exposed individuals can perform point-of-care tests more frequently compared with molecular tests, which often require visiting a facility, time-consuming off-site processing, or high cost.

Nucleic acid aptamers are short sequences of RNA or DNA that specifically bind target molecules and offer unique advantages over antibodies as molecular recognition agents for SARS-CoV-2. Aptamers can achieve specific binding to target molecules with affinities similar to antibodies.[5,6] Compared with protein antibodies, DNA aptamers are less expensive to synthesize, more stable, and more scalable for production. Because of these features, nucleic acid aptamers have been applied to a variety of fields, including therapeutics[7] and diagnostics.[8] A library selection method called systematic evolution of ligands by exponential enrichment (SELEX) is used to discover aptamer sequences.[9−11] A wide variety of selection targets can be used in SELEX, including whole cells[12] and proteins,[13] to yield highly specific and tight-binding aptamers. The spike (S) protein of SARS-CoV-2 is displayed on the viral surface and is therefore an attractive detection target for intact virus. The S protein is a homotrimer, and each monomer contains subunit 1 (S1) and subunit 2 (S2). Within S1, there are two distinct regions: the receptor-binding domain (RBD) and the N-terminal domain (NTD).[14,15] Several aptamers that bind SARS-CoV-2 S protein have been reported,[16−18] including the SARS-CoV-2 spike protein NTD-binding DNA aptamer 1 (SNAP1).[16]

Lateral flow assays (LFAs) are one type of diagnostic device that can provide rapid, point-of-care results. LFAs are not only fast, user-friendly, and convenient to use, but also inexpensive

Received: February 1, 2022
Accepted: April 10, 2022
Published: May 9, 2022

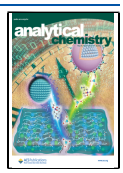

https://doi.org/10.1021/acs.analchem.2c00554
Anal. Chem. 2022, 94, 7278−7285

compared with lab tests. There are many commercial LFAs that test for diseases such as influenza, malaria, and HIV.[19] In addition to those applications, LFAs are also being applied to other areas, such as HIV drug resistance testing,[20−22] cancer biomarker screening,[23] and now COVID-19 testing.[24,25] Eight over-the-counter LFAs for COVID-19 were under emergency use authorization by the FDA as of November 2021.[2] These LFAs use protein antibodies to capture and detect nucleocapsid protein, which is highly conserved and abundant in samples.[26] However, nucleocapsid detection requires lysing the virus. Typically, patient swab samples are incubated in extraction buffer to release nucleocapsid and then used in testing assays. To streamline this process and eliminate this step, one strategy is to use a capture and detection agent that binds S protein instead of nucleocapsid protein. The S protein is also highly mutated among SARS-CoV-2 variants, so a multiplexed LFA that detects specific mutations in the S protein can be used to identify variants. In addition, replacing the antibodies with DNA aptamers could expedite to-scale production and reduce the cost of manufacturing.[27,28]

Previously, we demonstrated that SNAP1 binds to wild-type SARS-CoV-2 S protein with high affinity (<80 nM) and can detect UV-inactivated SARS-CoV-2 virus in a proof-of-concept LFA.[16] However, SNAP1 did not bind very well to S-2P, a stabilized form of the S protein. In this study, we implemented a hybrid SELEX strategy using S-2P expressed on cells and as purified proteins as selection targets. S-2P contains two stabilizing proline mutations and has been shown to better reflect its authentic topology in Cryo-EM studies. Therefore, SELEX utilizing S-2P may yield aptamers that bind more tightly to SARS-CoV-2 virus.[29,30] We discovered a new sequence named SARS-CoV-2 spike protein NTD-binding DNA aptamer 4 (SNAP4), which binds specifically to the NTD of S protein with <30 nM affinity. We employed SNAP4 and SNAP1 as capture and detection agents, respectively, in an aptamer sandwich LFA (AptaFlow). AptaFlow detected SARS-CoV-2 spike protein at 250 pM as well as UV-inactivated virus at 10^6 copies/mL, which recent findings suggest is sufficient to detect contagious users with high viral load.[31−33] AptaFlow takes <1 h to use and costs under $1 per test, demonstrating its potential as an accessible COVID-19 rapid test for detecting infectious individuals.

EXPERIMENTAL SECTION

Oligonucleotides. All oligonucleotides were synthesized by Integrated DNA Technologies. The ssDNA library used in the protein SELEX process was 5′-ATCCAGAGTGACG-CAGCA-N52-TGGACACGGTGGCTTAGT-3′. The forward primer for amplification was FAM-ATCCAGAGTGACGCAG, and the reverse primer for amplification was 5′-Biotin-GACACGGTGGCTTAGT-3′. Oligonucleotide sequences are listed in Table S2. Modifications to oligonucleotides included: FITC (5′- FITC − sequence −3′), biotin (5′-biotin−iSp18 spacer−sequence −3′), Cy5 (5′ − Cy5−sequence −3′), and thiol (5′- thiol−sequence −3′). All aptamer pools and aptamers were annealed before use in SELEX, binding, characterization, and other studies. Aptamers were annealed by diluting to 1−10 μM in SELEX WB (see buffers below), heating at 95 °C for 5 min, and snap-cooling on ice for at least 10 min.

Buffers. SELEX wash buffer (SELEX WB) contains 4.5 g/L glucose, 0.1 g/L $CaCl_2$, 0.2 g/L KCl, 0.2 g/L KH_2PO_4, 0.1 g/L $MgCl_2{\cdot}6H_2O$, 8 g/L NaCl, 2.1716 g/L Na_2HPO_4, and 5 mM $MgCl_2$. The buffer is filtered through a 0.22 μm sterile filter and stored at 4 °C. For binding buffers, yeast tRNA (Invitrogen) (tRNA), and salmon sperm DNA (Invitrogen) (SS DNA) are added to a final concentration of 0.1 mg/mL. Additionally, MACS BSA 10% stock solution (Miltenyi Biotec) is added to a 0.1−2% final concentration depending on the experiment.

Generation of HEK293_S-2P and Culturing Conditions. The HEK293 cell line was cultured in 1× DMEM (Gibco) containing 10% FBS. To generate the S-2P expressing cell line, HEK293 cells were nucleofected with SpeI (NEB) linearized plasmid SARS-CoV-2-FL_pseudo_2P_pcDNA3.1[29] using Cell Line Nucleofector Kit V (Lonza) according to the manufacturer's instructions. After 24 h, cells were subjected to G418 selection for 2 weeks to achieve stable integration. To enrich for high expressers, selected cells were incubated with 10 nM of biotinylated SNAP1 aptamer and antibiotin magnetic beads for 20 min then applied onto an MS column (Miltenyi Biotec). Expression was monitored with SARS-CoV-2 Spike Human anti-SARS-CoV-2, Alexa Fluor 488 (Novus Biologicals cat. no. NBP290980AF488) by flow cytometry.

Recombinant Proteins. SARS-CoV-2 S protein trimer S-2P was kindly provided by the Institute of Protein Design (IPD) at the University of Washington. SARS-CoV-2 S protein S1 domain (ACROBiosystems S1N−C5255), SARS-CoV-2 S protein trimer (ACROBiosystems SPN-C52H8), SARS-CoV-2 S protein S1 NTD (ACROBiosystems S1D-C52H6), SARS-CoV-2 S protein RBD (ACROBiosystems SPD-C5255), and CD8 protein (Sino Biologic 10980-H08H) were purchased in lyophilized form. All proteins contained the His-tag. These proteins were reconstituted, aliquoted, and stored according to manufacturer's recommendations. All proteins contained the His-tag.

Viruses. Inactivated SARS-CoV-2 virus samples at known concentrations were kindly provided by the NIH RADx-Radical Data Coordination Center (DCC) at the University of California San Diego and BEI Resources. UV-inactivated SARS-CoV-2 Isolate USA-WA1/2020 was measured to be at 4.5×10^7 copies of ORF1a/mL, with a limit of detection of 10^{-7} on the Roche Cobas 6800/8800 (qPCR) when tested immediately and of 10^{-2} on the BD Veritor (antigen testing) when tested immediately. Heat-inactivated SARS-CoV-2 Isolate USA-WA1/2020 was measured to be at 4.9×10^9 copies of ORF1a/mL, with a limit of detection of 10^{-9} on the Roche Cobas 6800/8800 (qPCR) when tested immediately and of 10^{-2} on the BD Veritor (antigen testing) when tested immediately. Virus samples used in this study have undergone at least one freeze−thaw cycle.

Protein-SELEX. The protocol was based on the guidelines outlined by Wang et al.[34] and is outlined in Figure 1. Experimental conditions for 10 rounds of SELEX are summarized in Table S1. For rounds 1−6, partitioning of bound and unbound aptamers was achieved by centrifugation of cells at 500 *x g* for 3 min. For rounds 7−10, aptamers were partitioned by Dynabeads His-tag isolation & Pulldown (Novex by Life Technologies) on a rack magnet. Aptamers were amplified with Phusion High-Fidelity DNA Polymerase (NEB). Annealing, strand separation, and composition of buffers were described previously.[12]

Next-Generation Sequencing (NGS) and Data Analysis. The DNA pools from SELEX rounds were PCR amplified with barcoded primers described in Table S3 using the MiSeq Reagent Kit v2 (300-cycles) (Illumina) and MiSeq System

https://doi.org/10.1021/acs.analchem.2c00554
Anal. Chem. 2022, 94, 7278−7285

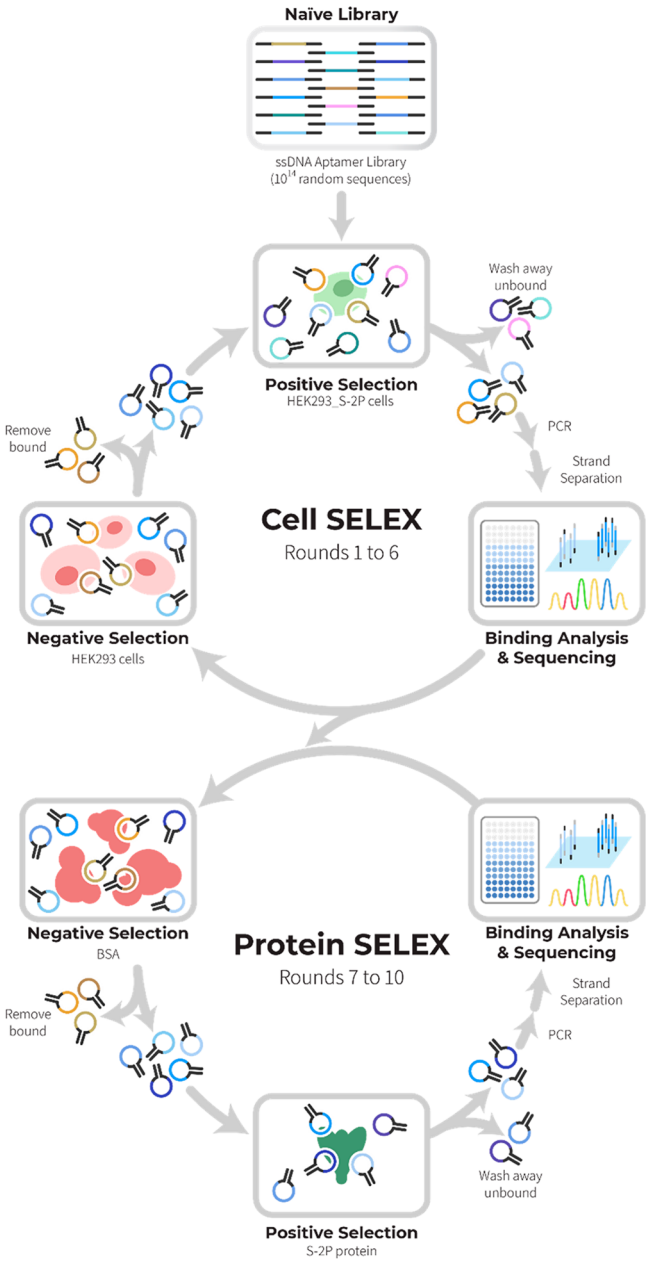

Figure 1. A naïve aptamer library is enriched for S-2P binders by cell SELEX and then protein SELEX. In cell SELEX, HEK293_S-2P cells are used for positive selection, and HEK293 cells are used for negative selection. In protein SELEX, S-2P recombinant protein is used for positive selection and bovine serum albumin (BSA) is used for negative selection. Aptamer pools are evaluated for binding to targets and sequenced.

(Illumina) per the manufacturer's protocol. Sequence reads were analyzed as previously described.[16] Secondary structure was predicted with NUPACK.[35]

Aptamer Binding Assay with Magnetic Spheres. Streptavidin or Protein G Sphero magnetic spheres (Spherotech) were used in binding assays. Streptavidin spheres were further modified with biotin anti-6-His epitope tag antibody (Biolegend cat. no. 906103). These spheres were used to immobilize SARS-CoV-2 S1-His and SARS-CoV-2 S1-Fc proteins, respectively. Individual Cy5 labeled aptamers were incubated with SARS-CoV-2 S1 spheres in binding buffer for 30 min at room temperature, washed twice with wash buffer (0.1% BSA, 0.01% Tween-20 SELEX WB), and analyzed by flow cytometry (Attune NxT, Invitrogen).

Biolayer Interferometry (BLI). Studies were performed with an Octet Red96 machine (Sartorius) at 25 °C and 1000 rpm sample agitation. Presoaked streptavidin (SA) sensors were rinsed in 1% BSA, 0.1 mg/mL tRNA, 0.1 mg/mL SS DNA, 0.01% Tween-20 SELEX WB ("diluent") for 100 s. Next, tips were loaded with 50 nM biotinylated aptamer until reaching a 0.5 nm signal threshold. Subsequently, tips were rinsed in diluent for 100 s and then baselined in diluent for another 100 s. After association with the protein of interest diluted to the desired concentration, sensor tips were returned to the baseline diluent well for dissociation. Data were analyzed with Octet Data Analysis 9.0 (Sartorius). Kinetic values were determined from a global fit of several curves generated from serial dilutions of the protein in a 1:1 or 1:2 binding model.

ELISA. Wells of a white streptavidin-coated 96-well plate (Thermo Fisher Scientific) were washed and blotted three times with SELEX WB and then incubated with 50 nM biotinylated NS or SNAP1 aptamer at 4 °C for 30 min. After three washes with wash buffer (0.1% Tween-20 2% BSA SELEX), wells were incubated with blocking buffer (5% BSA, 1:100 biotin blocking solution (Vector Laboratories), 0.1 mg/mL tRNA, 0.1 mg/mL SS DNA, and 0.1% Tween-20 SELEX WB) for 1.5 h at room temperature. Subsequently, the wells were incubated with S protein, UV-inactivated SARS-CoV-2 virus, or lentivirus in binding buffer (2% BSA, 0.1 mg/mL tRNA, 0.1 mg/mL SS DNA, 0.1% Tween-20 SELEX WB) for 30 min at room temperature. Then wells were washed four times before incubation with an anti-SARS-CoV-2 antibody with HRP (Novus Biologicals cat. no. NBP2−90980H). Lastly, wells were washed six times. All steps use 100 μL of the solution, except washing (200 μL of solution.) For wash steps, the plate is flicked over a sink and then blotted dry. Ice-cold ELISA Femto Substrate (Thermo Fisher Scientific) was added, and the plate luminescence was immediately measured by Infinite 200 PRO plate reader (Tecan) with 250 nm integration time and automatic attenuation.

Gold Nanoparticle Synthesis. Glassware and stir bar were cleaned thoroughly with aqua regia, rinsed with deionized water, and incubated at 80 °C overnight. Initially, 50 mL of 0.01% $HAuCl_4$ (Salt Lake Metals) was heated to boiling in a three-neck round-bottom flask with condenser. Then, 1 mL of 1% (34 mM) trisodium citrate was added. The solution was incubated for 15 min, gradually cooled to RT over several hours, and stored at 4 °C shielded from light. Nanoparticles were not used until at least 24 h after completion of synthesis and always sonicated before use. Particle size was checked by dynamic light scattering (DLS).

Gold Nanoparticle and Aptamer Conjugation. Protocol adapted from Liu and Lu.[36] Glass scintillation vials were incubated with 10 M NaOH for 1 h at RT and rinsed thoroughly with deionized water. Then 67.5 μL of thiolated aptamers were annealed at 10 μM in SELEX WB and then incubated with 6.75 μL of 500 mM acetate buffer (pH 5.2) and 10.13 μL of 10 mM freshly prepared TCEP for 1 h at RT. Gold nanoparticles (3 mL) were added to the glass vial, and then TCEP-treated aptamers were added dropwise. The solution was incubated at RT for at least 24 h with rocking shielded from light. Afterward, 30 μL of 500 mM Tris acetate (pH 8.2) and 300 μL of 1 M NaCl were added to the solution before incubation at RT for at least 24 h, shielded from light.

https://doi.org/10.1021/acs.analchem.2c00554
Anal. Chem. 2022, 94, 7278−7285

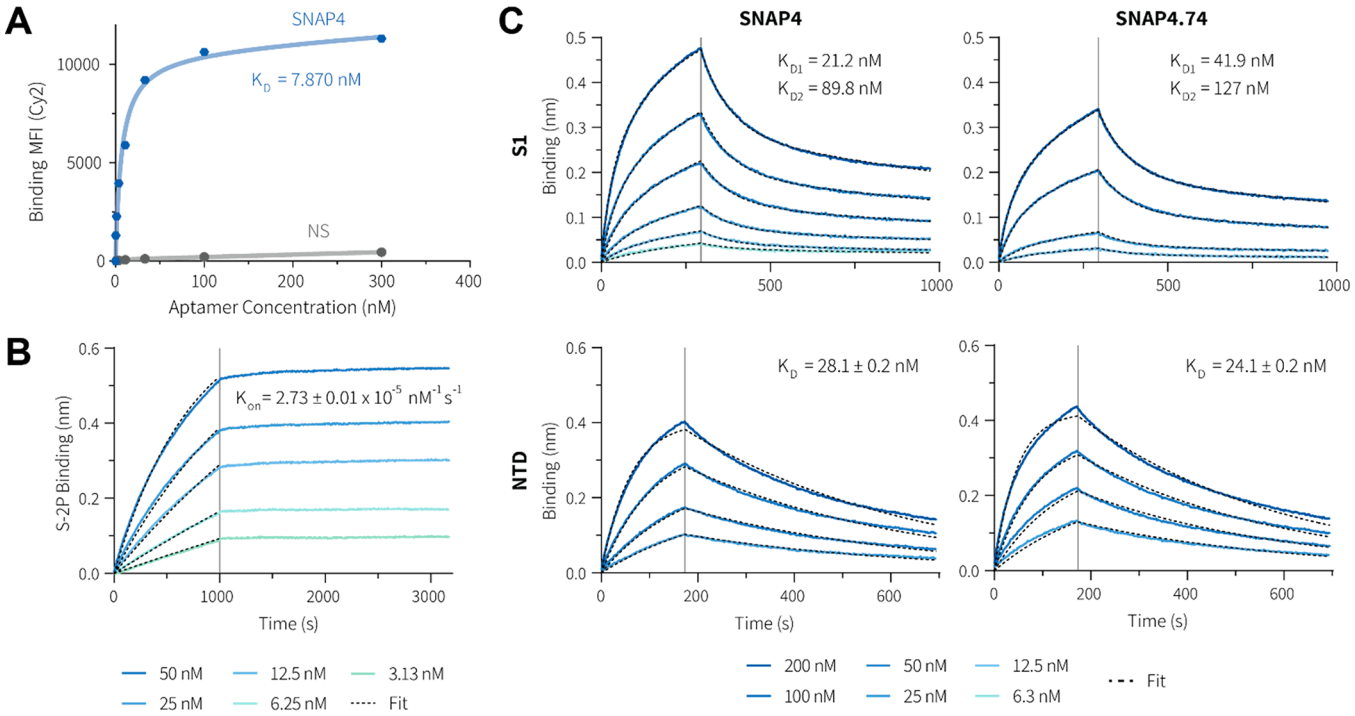

Figure 2. (A) Cy5-labeled SNAP4 at various concentrations was incubated with HEK293_S-2P cells to generate a binding curve. The graph shows the total (blue) and nonspecific (gray) binding of aptamer based on a one-site binding model (dashed lines). K_D was determined by nonlinear regression (1 biological replicate.) (B,C) Biotinylated aptamer was loaded on SA biosensors and associated with protein. The gray lines indicate the switch from analyte association to dissociation. K_{on} values (mean ± s.d., n = 4−6) were determined from a global fit (dark gray line) of the kinetic data at various concentrations of proteins for the indicated binding model. (B) SNAP4 aptamer binding to S-2P protein fitted to a 1:1 model for association only. (C) SNAP4 aptamer (left) or SNAP4.74 aptamer (right) binding to S1 protein with 1:2 model fit (top) or NTD protein with 1:1 model fit (bottom).

Aptamer-conjugated gold nanoparticles were stored at 4 °C shielded from light.

LFA Dipstick Manufacturing. The protocol was adapted from previous work.[21,22] Nitrocellulose membranes (Sartorius, 1UN95ER050030-B) assembled to a backing card (DCN, MIBA-020- 60 mm) were striped with test and control lines. Test line: 2 mg/mL polystreptavidin R (pSA) (Eagle Biosciences, # 10 120 030) in DPBS and control line: 0.6 mg/mL S-2P protein were striped at 1 μL/cm (Biodot, ZX1010), incubated at 37 °C for 30 min, and stored in the desiccated overnight at RT. Then, the card was attached to the absorbent pad (GE, 8117−2250) and sliced into 45 mm-width strips by the strip cutter (Kinbio, ZQ2000). Ponceau stain was used to stain the immobilized proteins to verify successful striped proteins as described previously.[20] Strips were stored in foil bags with desiccant at 4 °C until use.

Antibody-Free Aptamer LFA. Binding buffer (1% BSA, 0.1 mg/mL tRNA, 0.1 mg/mL SS DNA, 0.01% Tween-20), 25 nM biotinylated aptamer, and 50 μL of aptamer-functionalized gold nanoparticles were prepared, and then the analyte was added to a total volume of 100 μL. The solution was incubated at RT for 20 min with rocking. Then, a lateral flow device was dipped into the solution for 15−20 min (entire volume absorbed). Next, the lateral flow devices are dipped in 50 μL of SELEX WB for 5 min (partial volume absorbed). Lastly, the lateral flow devices were dipped in 50 μL of GoldEnhance (Nanoprobes) and developed over 10 min (entire volume absorbed). Test strips were photographed with a Galaxy S20 mobile phone (Samsung) and quantified on ImageJ. For each strip, the average pixel value in the control band, test band, and background (blank area between bands) was calculated. The control and test band values were background-subtracted, and then the ratio of test band:control band value was used. The LOD was determined from the lowest concentration of sample that was significantly higher than the negative control.

Nasal Swab Samples. Nasal swabs were obtained from healthy human volunteers. Nylon flocked dry swabs (Copan cat. no. 1C058S01) were fully inserted into a nostril and rotated in a circle 10 times, then repeated with the other nostril. Next, the swab was dipped into 1 mL SELEX WB, swirled vigorously, and spun at 8000g for 10 min.

RESULTS AND DISCUSSION

SELEX Strategy. We designed a selection strategy that combined cell and protein SELEX (Figure 1). For the first six rounds, we performed cell SELEX using S-2P-expressing cell line (HEK293_S-2P) as the binding target. Wild-type HEK293 cells were used in negative selection to reduce the binding of nonspecific sequences. We hypothesized that displaying S-2P on the cell membrane would provide a more authentic context for aptamer panning because the S protein is expressed on a lipid bilayer in the SARS-CoV-2 virus. The HEK293 cell line was chosen because it is commonly used for production of pseudovirus.[34] For rounds 7 to 10, we performed protein SELEX using S-2P recombinant protein as the target. We hypothesized that these rounds would select against aptamers that bind to proteins other than S-2P expressed on the cell surface. We increased selection pressure in sequential rounds of selection by tuning concentrations of aptamer pools, competitors, and ratios of cells and proteins used for positive

https://doi.org/10.1021/acs.analchem.2c00554
Anal. Chem. 2022, 94, 7278−7285

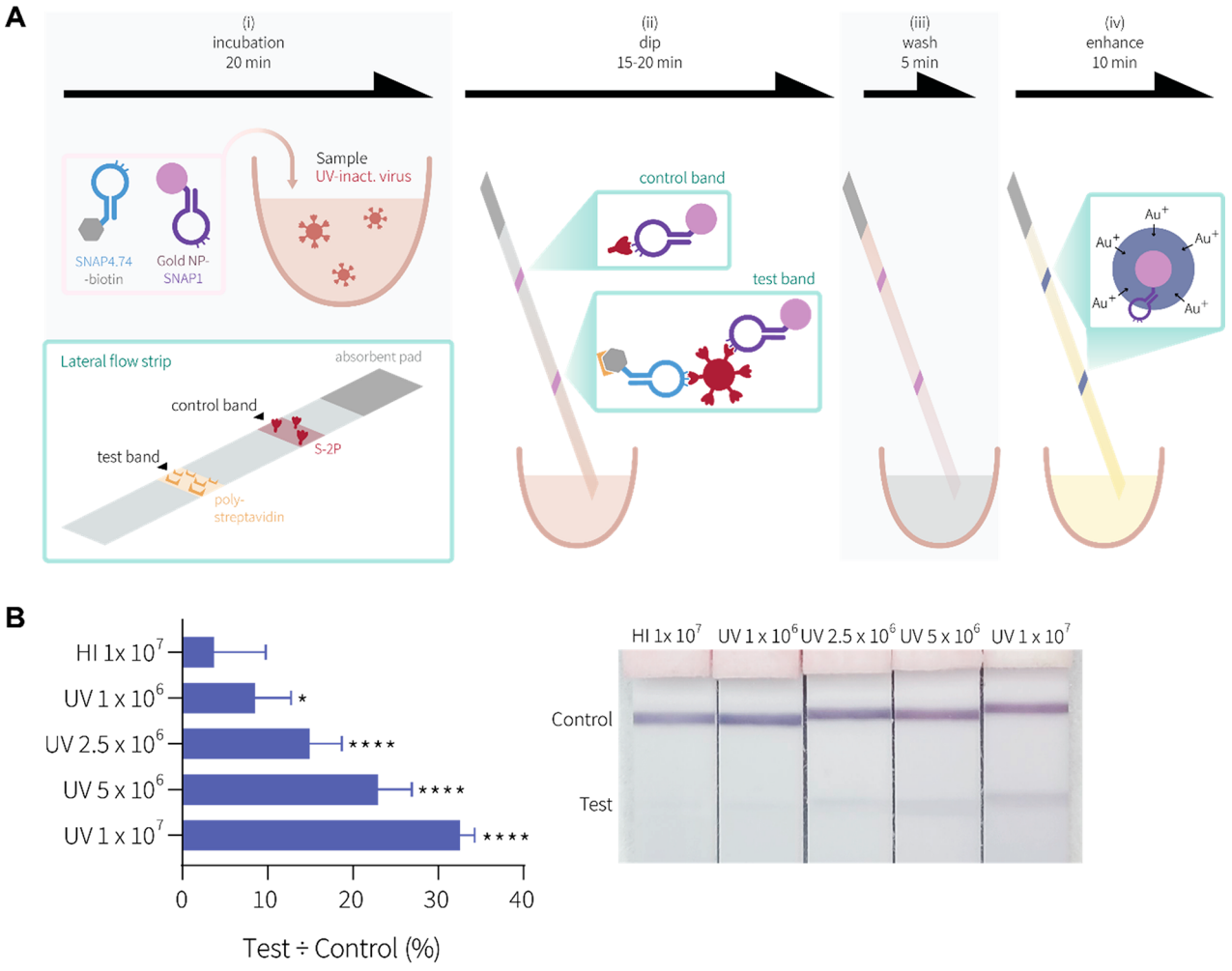

Figure 3. (A) Step-by-step process for AptaFlow. (i) incubating reagents with SARS-CoV-2 sample. (ii) dipping of the test strip into the sample. (iii) washing to reduce nonspecific signals. (iv) enhancing signal to increase sensitivity. (B) Limit of detection of LFA system with UV-inactivated virus (UV) at various concentrations (copies/mL) and heat-inactivated (HI) virus (negative control). Bars indicate mean. Brackets indicate 95% CI. Statistical significance was determined by one-way ANOVA with Dunnett correction. * indicates $p < 0.05$ and **** indicates $p < 0.0001$ when compared to HI 1×10^7 copies/mL; $n = 3–4$ per experimental group. A representative image is shown.

and negative selection according to Table S1. After observing increased binding of libraries from rounds 5 and 6 to HEK293_S-2P cells, we sequenced libraries from these rounds and identified one enriched sequence, A1, that bound the S-2P-expressing cells (Figure S1). We continued selection through protein SELEX, and characterized the resulting libraries by NGS analysis. We identified three additional candidate aptamers (A2, A3, and A4) as potential S-2P binders based on their prevalence (Table S2).

Aptamer Binding Characterization. We screened the four candidate aptamers by aptamer–antibody sandwich ELISA and found that A4 aptamer bound S-2P recombinant protein with the highest signal (Figure S2). To further characterize A4 aptamer, we used flow cytometry to quantify binding of the aptamer to HEK293_S-2P cells, which were used for positive selection in rounds 1–6 (Figure 2A). We measured an apparent K_D of 7.87 nM by fitting a binding curve to fluorescence measured at different A4 concentrations. Next, we monitored binding of A4 aptamer to immobilized S-2P protein using biolayer interferometry (Figure 2B). We measured an on-rate of $2.73 \pm 0.01 \times 10^{-5}$ nM^{-1} s^{-1} for A4 aptamer and S-2P. The off-rate was too low to measure, which may be due to multiple binding sites on trimeric S protein. Next, we narrowed down the binding location of A4 aptamer on S protein by measuring its binding affinity to S1 protein by BLI (Figure 2C, top left). The data best fit a 1:2 heterogeneous binding model, suggesting that the A4 aptamer may bind to more than one site on S protein. The K_{D1} was 21.2 ± 0.0 nM, and the K_{D2} was 89.8 ± 0.1 nM for A4 binding to S1 protein. We also tested binding to SARS-CoV-2 RBD by ELISA (Figure S2) and BLI (data not shown) and did not observe binding. Additionally, we measured the binding kinetics of A4 aptamer to the NTD of S protein (Figure 2C, bottom left). A4 aptamer bound NTD in a 1:1 manner with a K_D of 28.1 ± 0.2 nM. Notably, A4 aptamer's binding affinity for NTD is more than twice that of SNAP1 ($K_D = 60.4 \pm 1.6$ nM).[16] These data together demonstrate that A4 aptamer binds S-2P tightly at the NTD. Thus, we renamed A4 to SARS-CoV-2 spike protein NTD-binding DNA aptamer 4 (SNAP4).

Because of discovering several NTD-binding aptamers (SNAP1, SNAP3, and now SNAP4), we asked whether other S-binding aptamers also bound NTD,[12] including SP6.51 aptamer. SP6.51 was previously reported to bind the S protein in an RBD-independent manner.[17] We found that SP6.51 binds to S1 and NTD by BLI (Figure S3). We hypothesize that multiple independent SELEX processes have yielded NTD-

https://doi.org/10.1021/acs.analchem.2c00554
Anal. Chem. 2022, 94, 7278–7285

binding aptamers because the NTD is the most exposed part of the S protein. The NTD is the outermost region and exposed on all three monomers, unlike the RBD that can switch between a closed and open conformation and only 1 or 2 RBDs per spike protein are open.[14,35]

SNAP4 Aptamer Truncations. Truncations have been shown to improve binding affinity and decrease synthesis costs.[12,17] We designed two truncations of SNAP4 aptamer (88nt original length): SNAP4.74 (74nt in length) and SNAP4.40 (40nt in length) (Table S2). We predicted the secondary structure of SNAP4, SNAP4.74, and SNAP4.40 through the computational tool NUPACK[36] and observed similar core structures in the 52-nt random region (Figure S4A). We observed that SNAP4.74 binds similar targets and with similar affinity as SNAP4. SNAP4.74 bound S-2P and S1 in ELISA (Figure S4B) and bound S1 and NTD with kinetic constants in the same range as those of SNAP4 (Figure 2C, right half). We did not observe binding of SNAP4.40 aptamer to S-2P and S1 protein by ELISA and BLI (Figure S4B). Overall, the high affinity of SNAP4 and SNAP4.74 aptamer for S-2P-expressing cells as well as S-2P protein shows that the cell and protein SELEX strategy enriched for a robust, target-binding aptamer.

SNAP1 and SNAP4 Competition Study. To determine whether SNAP1 and SNAP4 compete for the same binding site and can be used together in detection assays, we incubated various ratios of unlabeled aptamer to fluorescently labeled Cy5-SNAP1 and measured binding of Cy5-SNAP1 to immobilized S1 protein by flow cytometry. As expected, unlabeled SNAP1 effectively reduced binding of Cy5-SNAP1 to S1 protein (Figure S5). In contrast, there was no significant difference in Cy5-SNAP1 binding to S1 protein in the presence of either unlabeled scrSNAP1, an aptamer that does not bind S protein, and unlabeled SNAP4.74 at ratios of 10:1 and 20:1. These data support that SNAP1 and SNAP4.74 have minimal competition and are suitable to use together.

Aptamer Sandwich LFA (AptaFlow). To apply SNAP4 to SARS-CoV-2 testing, we developed an antibody-free aptamer-based lateral flow assay (AptaFlow) (Figure 3A). We use biotinylated aptamer for analyte capture onto streptavidin-coated test band, and aptamer-conjugated gold nanoparticles for detection. First, all components, including analyte, biotinylated aptamer, and aptamer-conjugated gold nanoparticles, are incubated together. A lateral flow strip is dipped sequentially into the sample, wash buffer, and signal enhancing buffer. In total, the assay takes under 1 h to complete. First, we tested whether AptaFlow could detect S-2P protein. We found that AptaFlow that used SNAP4.74-gold nanoparticles and SNAP4.74-biotin were highly sensitive, detecting as low as 100 pM S-2P protein (Figure S6). We were able to detect as low as 500 pM S-2P protein spiked in healthy human volunteer nasal swab samples using AptaFlow with SNAP1-gold nanoparticles and SNAP4.74-biotin (Figure S7), indicating that our system can detect S protein in clinically relevant samples.

We validated that both SNAP1[16] and SNAP4 can detect UV-inactivated SARS-CoV-2 in aptamer−antibody sandwich ELISAs. Therefore, we hypothesized that SNAP1 and SNAP4.74 can be used in AptaFlow to detect UV-inactivated virus. First, we compared how well SNAP4.74- and SNAP1-conjugated gold nanoparticles can detect UV-inactivated SARS-CoV-2 virus. We found that AptaFlow using SNAP4.74-conjugated gold nanoparticles and SNAP4.74-biotin did not detect virus at 1×10^7 copies/mL. However, AptaFlow using SNAP1-conjugated gold nanoparticles and SNAP4.74-biotin gave an 8.7-fold higher signal for 1×10^7 copies/mL UV-inactivated virus than the equivalent concentration of our negative control, heat-inactivated virus. We previously showed that heat-inactivated virus, which contained denatured S protein, is not recognized by SNAP1.[16] AptaFlow using SNAP1-conjugated gold nanoparticles and SNAP4.74-biotin can detect UV-inactivated virus at concentrations as low as 10^6 copies/mL (Figure 3B).

In this application, AptaFlow required two different aptamer sequences with different epitopes to detect low concentrations of virus despite the trimeric nature of S protein and its multivalent display on SARS-CoV-2. It is possible that when the analyte is very limited, the sterically unhindered biotinylated aptamer binds to the majority of potential sites on one analyte molecule, preventing the gold nanoparticle-conjugated aptamer from binding. Using minimally competing aptamers such as SNAP1 and SNAP4.74 could avoid this limitation.

AptaFlow detected 100 pM S protein, which is equivalent to approximately 6×10^9 S protein in sample, but AptaFlow also detected 10^6 copies/mL virus, which is approximately 2×10^6 S protein in a sample (assuming ~20 S protein per virus[37]). The higher sensitivity with virus samples may be due to only needing one or few capture aptamers to anchor the virus particle onto the test band, allowing the majority of the other binding sites to be occupied by the detection aptamer.

CONCLUSION

In this article, we discovered and characterized SNAP4, a DNA aptamer that binds the SARS-CoV-2 S protein at the NTD. Using SNAP4 and SNAP1, we developed an aptamer sandwich LFA (AptaFlow) with a LOD for UV-inactivated virus of 10^6 copies/mL, which is the minimal LOD set by the WHO.[38] Compared with other antigen tests, AptaFlow theoretically outperforms 5 out of 18 commercially available tests.[38] Recent findings suggest that individuals with low viral loads of $<10^6$ copies/mL are unlikely to transmit the disease,[31−33,39] suggesting that antigen tests like AptaFlow can be used to detect infectious cases. Additionally, AptaFlow provides results in under 1 h and costs under $1 per test to manufacture in our hands. AptaFlow can be further improved by (1) integrating gold nanoparticles and biotinylated aptamer onto sample pad of lateral flow strip to eliminate one step and save 20 min; (2) using complementary DNA in the control band instead of S-2P protein to reduce costs and improve scalability; and (3) utilize multiple capture aptamers that bind to different mutation epitopes, which may allow detection of different variants. Although SARS-CoV-2 rapidly mutates and AptaFlow best detects the wild-type virus, SNAP1 and SNAP4 are modular and can be substituted with new aptamer sequences that detect other variants. By enabling more frequent at-home testing, more accessible diagnostic tools like AptaFlow may reduce the burden of the COVID-19 pandemic on healthcare systems.

ASSOCIATED CONTENT

Supporting Information

The Supporting Information is available free of charge at https://pubs.acs.org/doi/10.1021/acs.analchem.2c00554.

Sequences and supplementary experiments (PDF)

https://doi.org/10.1021/acs.analchem.2c00554
Anal. Chem. 2022, 94, 7278−7285

AUTHOR INFORMATION

Corresponding Author

Suzie H. Pun − *Department of Bioengineering and Molecular Engineering and Sciences Institute, University of Washington, Seattle, Washington 98195, United States;* orcid.org/0000-0003-1443-4996; Email: spun@uw.edu

Authors

Lucy F. Yang − *Department of Bioengineering and Molecular Engineering and Sciences Institute, University of Washington, Seattle, Washington 98195, United States*

Nataly Kacherovsky − *Department of Bioengineering and Molecular Engineering and Sciences Institute, University of Washington, Seattle, Washington 98195, United States*

Nuttada Panpradist − *Department of Bioengineering and Molecular Engineering and Sciences Institute, University of Washington, Seattle, Washington 98195, United States;* orcid.org/0000-0002-2733-4110

Ruixuan Wan − *Department of Chemistry, University of Washington, Seattle, Washington 98195, United States;* orcid.org/0000-0001-6135-3166

Joey Liang − *Department of Bioengineering and Molecular Engineering and Sciences Institute, University of Washington, Seattle, Washington 98195, United States*

Bo Zhang − *Department of Chemistry, University of Washington, Seattle, Washington 98195, United States;* orcid.org/0000-0002-1737-1241

Stephen J. Salipante − *Department of Laboratory Medicine, University of Washington, Seattle, Washington 98195, United States*

Barry R. Lutz − *Department of Bioengineering and Molecular Engineering and Sciences Institute, University of Washington, Seattle, Washington 98195, United States*

Complete contact information is available at: https://pubs.acs.org/10.1021/acs.analchem.2c00554

Author Contributions

The manuscript was written through contributions of all authors. All authors have given approval to the final version of the manuscript.

Funding

This work was supported by NIH 1U01AA029316.

Notes

The authors declare no competing financial interest.

ACKNOWLEDGMENTS

We thank NIH RADx-Radical Data Coordination Center (DCC) at University of California San Diego (funded under NIH grant no. 1U24LM013755-01) for the SARS-Related Coronavirus 2, Isolate USA-WA1/2020, NR-52281 deposited by the Centers for Disease Control and Prevention and obtained through BEI Resources, NIAID. We thank Lexi Walls and Dr. David Veesler for providing the SARS-CoV-2-FL_pseudo_2P_pcDNA3.1 plasmid, Lauren Carter from the Institute of Protein Design (IPD) who kindly produced S-2P protein through support from the Bill and Melinda Gates Foundation, Kelsi Penewit for NGS assistance, and Daniel Leon for lateral flow strip manufacturing assistance.

REFERENCES

(1) Wouters, O. J.; Shadlen, K. C.; Salcher-Konrad, M.; Pollard, A. J.; Larson, H. J.; Teerawattananon, Y.; Jit, M. *Lancet* **2021**, *397* (10278), 1023−1034.

(2) Peeling, R. W.; Olliaro, P. L.; Boeras, D. I.; Fongwen, N. *Lancet Infect. Dis* **2021**, *21* (9), e290−e295.

(3) Larremore, D. B.; Wilder, B.; Lester, E.; Shehata, S.; Burke, J. M.; Hay, J. A.; Milind, T.; Mina, M. J.; Parker, R. Test sensitivity is secondary to frequency and turnaround time for COVID-19 surveillance. *medRxiv*, September 8, **2020**. DOI: 10.1101/2020.06.22.20136309.

(4) Mina, M. J.; Parker, R.; Larremore, D. B. *N. Engl. J. Med.* **2020**, *383* (22), No. e120.

(5) Nimjee, S. M.; Rusconi, C. P.; Sullenger, B. A. *Annu. Rev. Med.* **2005**, *56* (1), 555−583.

(6) Bunka, D. H. J.; Stockley, P. G. *Nat. Rev. Microbiol* **2006**, *4* (8), 588−596.

(7) Keefe, A. D.; Pai, S.; Ellington, A. *Nat. Rev. Drug Discov* **2010**, *9* (7), 537−550.

(8) Kumar Kulabhusan, P.; Hussain, B.; Yüce, M. *Pharmaceutics* **2020**, *12* (7), 646.

(9) Tuerk, C.; Gold, L. *Science* **1990**, *249* (4968), 505−510.

(10) Ellington, A. D.; Szostak, J. W. *Nature* **1990**, *346* (6287), 818−822.

(11) Robertson, D. L.; Joyce, G. F. *Lett. Nat.* **1990**, *344* (March), 467−468.

(12) Kacherovsky, N.; Cardle, I. I.; Cheng, E. L.; Yu, J. L.; Baldwin, M. L.; Salipante, S. J.; Jensen, M. C.; Pun, S. H. *Nat. Biomed. Eng.* **2019**, *3* (10), 783−795.

(13) Gotrik, M. R.; Feagin, T. A.; Csordas, A. T.; Nakamoto, M. A.; Soh, H. T. *Acc. Chem. Res.* **2016**, *49* (9), 1903−1910.

(14) Li, F. *Annu. Rev. Virol* **2016**, *3*, 237−261.

(15) McCallum, M.; Walls, A. C.; Bowen, J. E.; Corti, D.; Veesler, D. *Nat. Struct. Mol. Biol.* **2020**, *27*, 942−949.

(16) Kacherovsky, N.; Yang, L. F.; Dang, H. V.; Cheng, E. L.; Cardle, I. I.; Walls, A. C.; McCallum, M.; Sellers, D. L.; DiMaio, F.; Salipante, S. J.; Corti, D.; Veesler, D.; Pun, S. *Angew. Chem. Int. Ed* **2021**, *60*, 21211−21215.

(17) Schmitz, A.; Weber, A.; Bayin, M.; Breuers, S.; Fieberg, V.; Famulok, M.; Mayer, G. *Angew. Chem. - Int. Ed* **2021**, *60*, 10279−10285.

(18) Song, Y.; Song, J.; Wei, X.; Huang, M.; Sun, M.; Zhu, L.; Lin, B.; Shen, H.; Zhu, Z.; Yang, C. *Anal. Chem.* **2020**, *92* (14), 9895−9900.

(19) Posthuma-Trumpie, G. A.; Korf, J.; van Amerongen, A. *Anal. Bioanal. Chem.* **2009**, *393* (2), 569−582.

(20) Panpradist, N.; Beck, I. A.; Chung, M. H.; Kiarie, J. N.; Frenkel, L. M.; Lutz, B. R. *PLoS One* **2016**, *11* (1), No. e0145962.

(21) Panpradist, N.; Beck, I. A.; Vrana, J.; Higa, N.; McIntyre, D.; Ruth, P. S.; So, I.; Kline, E. C.; Kanthula, R.; Wong-On-Wing, A.; Lim, J.; Ko, D.; Milne, R.; Rossouw, T.; Feucht, U. D.; Chung, M.; Jourdain, G.; Ngo-Giang-Huong, N.; Laomanit, L.; Soria, J.; Lai, J.; Klavins, E. D.; Frenkel, L. M.; Lutz, B. R. *EBioMedicine* **2019**, *50*, 34−44.

(22) Panpradist, N.; Beck, I. A.; Ruth, P. S.; Ávila-Ríos, S.; García-Morales, C.; Soto-Nava, M.; Tapia-Trejo, D.; Matías-Florentino, M.; Paz-Juarez, H. E.; Del Arenal-Sanchez, S.; Reyes-Terán, G.; Lutz, B. R.; Frenkel, L. M. *AIDS London Engl* **2020**, *34* (9), 1331−1338.

(23) Mahmoudi, T.; de la Guardia, M.; Baradaran, B. *TrAC Trends Anal. Chem.* **2020**, *125*, 115842.

(24) Grant, B. D.; Anderson, C. E.; Williford, J. R.; Alonzo, L. F.; Glukhova, V. A.; Boyle, D. S.; Weigl, B. H.; Nichols, K. P. *Anal. Chem.* **2020**, *92* (16), 11305−11309.

(25) Panpradist, N.; Kline, E. C.; Atkinson, R. G.; Roller, M.; Wang, Q.; Hull, I. T.; Kotnik, J. H.; Oreskovic, A. K.; Bennett, C.; Leon, D.; Lyon, V.; Gilligan-Steinberg, S. D.; Han, P. D.; Drain, P. K.; Starita, L. M.; Thompson, M. J.; Lutz, B. R. *Sci. Adv.* **2021**, *7*, eabj1281.

(26) Oliveira, S. C.; de Magalhães, M. T. Q.; Homan, E. J. *Front. Immunol* **2020**, *11*, 587615.

(27) Lakhin, A. V.; Tarantul, V. Z.; Gening, L. V. *Acta Naturae* **2013**, *5* (4), 34−43.
(28) Baker, B. R.; Lai, R. Y.; Wood, M. S.; Doctor, E. H.; Heeger, A. J.; Plaxco, K. W. *J. Am. Chem. Soc.* **2006**, *128* (10), 3138−3139.
(29) Wrapp, D.; Wang, N.; Corbett, K. S.; Goldsmith, J. A.; Hsieh, C. L.; Abiona, O.; Graham, B. S.; McLellan, J. S. *Science* **2020**, *367* (6483), 1260−1263.
(30) Hsieh, C.; Goldsmith, J. A.; Schaub, J. M.; Divenere, A. M.; Kuo, H.; Javanmardi, K.; Le, K. C.; Wrapp, D.; Lee, A. G.; Liu, Y.; Chou, C.; Byrne, P. O.; Hjorth, C. K.; Johnson, N. V.; Ludes-meyers, J.; Nguyen, A. W.; Park, J.; Wang, N.; Amengor, D.; Lavinder, J. J.; Ippolito, G. C.; Maynard, J. A.; Finkelstein, I. J.; Mclellan, J. S. *Science* **2020**, *369* (6510), 1501−1505.
(31) COVID-19 Target product profiles for priority diagnostics to support response to the COVID-19 pandemic v.1.0, 2020. https://www.who.int/publications/m/item/covid-19-target-product-profiles-for-priority-diagnostics-to-support-response-to-the-covid-19-pandemic-v.0.1 (accessed March 28, 2022).
(32) Cubas-Atienzar, A. I.; Kontogianni, K.; Edwards, T.; Wooding, D.; Buist, K.; Thompson, C. R.; Williams, C. T.; Patterson, E. I.; Hughes, G. L.; Baldwin, L.; Escadafal, C.; Sacks, J. A.; Adams, E. R. *Sci. Rep* **2021**, *11* (1), 18313.
(33) Wölfel, R.; Corman, V. M.; Guggemos, W.; Seilmaier, M.; Zange, S.; Müller, M. A.; Niemeyer, D.; Jones, T. C.; Vollmar, P.; Rothe, C.; Hoelscher, M.; Bleicker, T.; Brünink, S.; Schneider, J.; Ehmann, R.; Zwirglmaier, K.; Drosten, C.; Wendtner, C. *Nature* **2020**, *581* (7809), 465−469.
(34) Wang, T.; Yin, W.; AlShamaileh, H.; Zhang, Y.; Tran, P. H.-L.; Nguyen, T. N.-G.; Li, Y.; Chen, K.; Sun, M.; Hou, Y.; Zhang, W.; Zhao, Q.; Chen, C.; Zhang, P.-Z.; Duan, W. *Hum. Gene Ther. Methods* **2019**, *30* (1), 1−16.
(35) Zadeh, J. N.; Steenberg, C. D.; Bois, J. S.; Wolfe, B. R.; Pierce, M. B.; Khan, A. R.; Dirks, R. M.; Pierce, N. A. *J. Comput. Chem.* **2011**, *32* (1), 170−173.
(36) Liu, J.; Lu, Y. *Nat. Protoc* **2006**, *1* (1), 246−252.
(37) Ke, Z.; Oton, J.; Qu, K.; Cortese, M.; Zila, V.; McKeane, L.; Nakane, T.; Zivanov, J.; Neufeldt, C. J.; Cerikan, B.; Lu, J. M.; Peukes, J.; Xiong, X.; Kräusslich, H.-G.; Scheres, S. H. W.; Bartenschlager, R.; Briggs, J. A. G. *Nature* **2020**, *588* (7838), 498−502.
(38) Alemany, A.; Baró, B.; Ouchi, D.; Rodó, P.; Ubals, M.; Corbacho-Monné, M.; Vergara-Alert, J.; Rodon, J.; Segalés, J.; Esteban, C.; Fernández, G.; Ruiz, L.; Bassat, Q.; Clotet, B.; Ara, J.; Vall-Mayans, M.; G-Beiras, C.; Blanco, I.; Mitjà, O. *J. Infect* **2021**, *82* (5), 186−230.
(39) Singanayagam, A.; Patel, M.; Charlett, A.; Bernal, J. L.; Saliba, V.; Ellis, J.; Ladhani, S.; Zambon, M.; Gopal, R. *Eurosurveillance* **2020**, *25* (32), 2001483.

https://doi.org/10.1021/acs.analchem.2c00554
Anal. Chem. 2022, 94, 7278−7285